

University of Nebraska - Lincoln

DigitalCommons@University of Nebraska - Lincoln

Mechanical & Materials Engineering Faculty
Publications

Mechanical & Materials Engineering,
Department of

8-2-2022

Vibrating Flexoelectric Micro-Beams as Angular Rate Sensors

Yilin Qu

Feng Jin

Jiashi S. Yang

Follow this and additional works at: <https://digitalcommons.unl.edu/mechengfacpub>




Part of the [Mechanics of Materials Commons](#), [Nanoscience and Nanotechnology Commons](#), [Other Engineering Science and Materials Commons](#), and the [Other Mechanical Engineering Commons](#)

This Article is brought to you for free and open access by the Mechanical & Materials Engineering, Department of at DigitalCommons@University of Nebraska - Lincoln. It has been accepted for inclusion in Mechanical & Materials Engineering Faculty Publications by an authorized administrator of DigitalCommons@University of Nebraska - Lincoln.

Article

Vibrating Flexoelectric Micro-Beams as Angular Rate Sensors

Yilin Qu ¹, Feng Jin ^{1,*} and Jiashi Yang ^{2,*} 

¹ State Key Laboratory for Strength and Vibration of Mechanical Structures, Xi'an Jiaotong University, Xi'an 710049, China; 18229058666@163.com

² Department of Mechanical and Materials Engineering, University of Nebraska-Lincoln, Lincoln, NE 68588-0526, USA

* Correspondence: jinfengzhao@263.net (F.J.); jyang1@unl.edu (J.Y.)

Abstract: We studied flexoelectrically excited/detected bending vibrations in perpendicular directions of a micro-beam spinning about its axis. A set of one-dimensional equations was derived and used in a theoretical analysis. It is shown that the Coriolis effect associated with the spin produces an electrical output proportional to the angular rate of the spin when it is small. Thus, the beam can be used as a gyroscope for angular rate sensing. Compared to conventional piezoelectric beam gyroscopes, the flexoelectric beam proposed and analyzed has a simpler structure.

Keywords: gyroscope; flexoelectric; beam; vibration



Citation: Qu, Y.; Jin, F.; Yang, J. Vibrating Flexoelectric Micro-Beams as Angular Rate Sensors. *Micromachines* **2022**, *13*, 1243. <https://doi.org/10.3390/mi13081243>

Academic Editor: Seung-bok Choi

Received: 20 June 2022

Accepted: 31 July 2022

Published: 2 August 2022

Publisher's Note: MDPI stays neutral with regard to jurisdictional claims in published maps and institutional affiliations.



Copyright: © 2022 by the authors. Licensee MDPI, Basel, Switzerland. This article is an open access article distributed under the terms and conditions of the Creative Commons Attribution (CC BY) license (<https://creativecommons.org/licenses/by/4.0/>).

1. Introduction

Gyroscopes are key components for motion sensing. Early gyroscopes were based on the inertia of a rotating rigid body. Later, vibratory and optical gyroscopes were subsequently developed. This paper is concerned with vibratory gyroscopes in which vibrations are usually excited and detected piezoelectrically or electrostatically. The literature on vibratory gyroscopes is numerous. Early references can be found in a few review articles [1–3] and Ph.D. dissertations [4,5]. Relatively recent ones are, e.g., [6–10], among which, [10] is a review on micromachined and nano gyroscopes.

Specifically, for piezoelectric vibratory gyroscopes based on flexural vibrations of thin beams [11], since piezoelectric coupling produces strains rather than curvatures, either a composite beam or some complicated electrode configuration is typically needed to excite and detect flexural motions of beams [11–13].

Recently, there has been a growing interest in the flexoelectric effect [14–17], with which, flexural motion in a homogeneous beam [18–20] or plate [21] can be excited or detected with only electrodes. In particular, flexoelectric beams have already been used as actuators or sensors in electromechanical devices [22,23]. This offers the possibility of flexoelectric angular rate sensors. In this paper, we propose a flexoelectric beam vibratory gyroscope that is original. The flexoelectric beam in the proposed gyroscope functions as both an actuator and a sensor at the same time through two pairs of electrodes and flexural vibrations in perpendicular directions. We demonstrate how the proposed gyroscope works through modeling. The basic three-dimensional theory of flexoelectricity is gathered in Section 2, from which, a one-dimensional model for flexural motions of the gyroscope is established in Section 3. A theoretical analysis and numerical results are presented in Sections 4 and 5, respectively, to show the basic response of the beam when it is rotating about its axis. Finally, some conclusions are drawn in Section 6.

2. Theory of Flexoelectricity

The macroscopic theory of flexoelectricity [15–17] is summarized below for its notation. It is also the foundation for the one-dimensional (1-D) model to be developed in the next section. In Cartesian tensor notation [24], the field equations are

$$T_{ij,j} - \tau_{ijk,jk} + F_i = \rho \ddot{u}_i, \tag{1a}$$

$$D_{i,i} = 0, \tag{1b}$$

where \mathbf{T} is the stress tensor, $\boldsymbol{\tau}$ a higher-order stress, \mathbf{F} the body force vector, ρ the mass density, which is a scalar, \mathbf{u} the mechanical displacement vector, and \mathbf{D} the electric displacement vector. A vector or tensor is written either in boldface or in component form with one index (vector) or more indices (tensor) [24]. A comma followed by an index denotes partial differentiation with respect to the coordinate associated with the index [24]. We limit ourselves to nonpiezoelectric materials. The constitutive relations accompanying Equation (1) describing material behaviors are

$$\begin{aligned} T_{ij} &= C_{ijkl}S_{kl}, \quad \tau_{ijk} = -f_{ijk}E_l, \\ D_i &= \varepsilon_{ij}E_j + f_{ijkl}\eta_{jkl}, \end{aligned} \tag{2}$$

where \mathbf{S} is the strain tensor, \mathbf{E} the electric field vector, $\boldsymbol{\eta}$ the strain gradient tensor, C_{ijkl} the elastic stiffness tensor, f_{ijkl} the flexoelectric constants (tensor), and ε_{ij} the dielectric constants (tensor). \mathbf{S} , $\boldsymbol{\eta}$, and \mathbf{E} are related to \mathbf{u} and the scalar electric potential ϕ through

$$S_{ij} = (u_{i,j} + u_{j,i})/2, \quad \eta_{jkl} = S_{jk,l}, \quad E_i = -\phi_{,i}. \tag{3}$$

3. One-Dimensional Equations for a Flexoelectric Beam in Bending Vibrations

Consider the thin flexoelectric beam in Figure 1. Its lateral surfaces are traction free and are electroded. The voltage across the two electrodes at $x_2 = \pm a$ for actuation is $V_2(t)$, and that between the two electrodes at $x_3 = \pm b$ for sensing is $V_3(t)$.

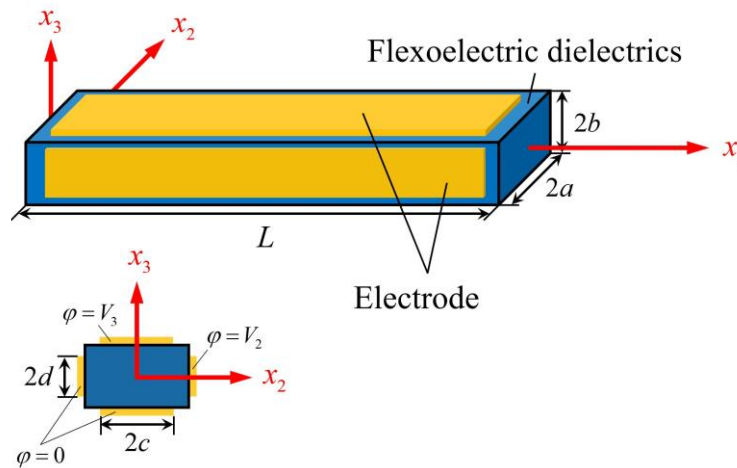


Figure 1. A thin flexoelectric beam and coordinate system whose origin is at the center of the left face.

1-D equations for bending in the (x_1, x_3) plane were derived from Equations (1)–(3) in [20]. For the gyroscope application to be studied in the next section, we need to generalize the 1-D equations in [20] to the case of simultaneous bending in both of the (x_1, x_2) and (x_1, x_3) planes. In this case, the displacement components are approximated by

$$\begin{aligned} u_2 &\cong u_2(x_1, t), \quad u_3 \cong u_3(x_1, t), \\ u_1 &\cong -x_2 u_{2,1} - x_3 u_{3,1}, \end{aligned} \tag{4}$$

which produce the following axial strain and strain gradients:

$$\begin{aligned} S_{11} &= -x_2 u_{2,11} - x_3 u_{3,11}, \\ \eta_{112} &= -u_{2,11}, \quad \eta_{113} = -u_{3,11}. \end{aligned} \tag{5}$$

Since the lateral surfaces of the beam are electroded and the electric potential are functions of time only on ideal electrodes that we assume, the electric field is approximated by

$$E_2 = -\frac{V_2}{2a}, \quad E_3 = -\frac{V_3}{2b}, \quad E_1 = 0. \tag{6}$$

The equations for bending are obtained by integrating Equation (1a) with $i = 2$ and 3 over the beam cross section, which results in [20]

$$\begin{aligned} Q_{2,1} + f_2 A &= \rho A \ddot{u}_2, \\ Q_{3,1} + f_3 A &= \rho A \ddot{u}_3, \end{aligned} \tag{7}$$

where Q_2 and Q_3 are the transverse shear forces in the x_2 and x_3 directions, respectively, and $A = 4ab$ is the area of the beam cross section. The integration of the products of Equation (1a) with x_2 or x_3 over the beam cross section yields the following shear force-bending moment relation [20]:

$$Q_2 = M_{3,1}, \quad Q_3 = M_{2,1} \tag{8}$$

where M_3 and M_2 are moments associated with bending in the (x_1, x_2) and (x_1, x_3) planes, respectively. For thin beams, the rotatory inertia is neglected. The 1-D constitutive relations are obtained by integrating the relevant equations in Equation (2) and their products with x_2 or x_3 over a cross section. The results are

$$M_3 = -\bar{c} B_2 u_{2,11} - f_{3113} A E_2, \tag{9a}$$

$$M_2 = -\bar{c} B_3 u_{3,11} - f_{3113} A E_3, \tag{9b}$$

$$D_2^{(0)} = \varepsilon_{11} A E_2 - f_{3113} A u_{2,11}, \tag{9c}$$

$$D_3^{(0)} = \varepsilon_{11} A E_3 - f_{3113} A u_{3,11}, \tag{9d}$$

where

$$\begin{aligned} \bar{c} &= \frac{(c_{1111} - c_{1122})(c_{1111} + 2c_{1122})}{c_{1111} + c_{1122}}, \\ B_2 &= \int_A x_2^2 dA, \quad B_3 = \int_A x_3^2 dA. \end{aligned} \tag{10}$$

$D_2^{(0)}$ and $D_3^{(0)}$ are needed to calculate the charge on the electrodes. Substitutions from Equations (8) and (9), we can write Equation (7) as two equations for u_1 and u_2 :

$$\begin{aligned} -\bar{c} B_2 u_{2,1111} + F_2 A &= \rho A \ddot{u}_2, \\ -\bar{c} B_3 u_{3,1111} + F_3 A &= \rho A \ddot{u}_3. \end{aligned} \tag{11}$$

4. Analysis of a Flexoelectric Gyroscope

When the beam in Figure 1 is used as a gyroscope, it is rotating about the x_1 axis with an angular rate Ω that is to be measured. We fixed the coordinate system to the rotating beam. In the rotating coordinate system, the effects of the centripetal and Coriolis accelerations can be taken into consideration through the following effective forces:

$$\begin{aligned} F_2 &= -\rho(-2\Omega \dot{u}_3 - \Omega^2 u_2), \\ F_3 &= -\rho(2\Omega \dot{u}_2 - \Omega^2 u_3). \end{aligned} \tag{12}$$

V_2 is the known applied voltage that drives the beam into bending with u_2 . The effective Coriolis force then drives the beam into bending with u_3 , which produces V_3 , which is unknown. The charge on the electrode at $x_3 = b$ is given by

$$Q^e = 2c \int_0^L -D_3|_{x_3=b} dx_1 = \frac{2cL\epsilon_{11}V_3}{2b} + 2cf_{3113}[u_{3,1}(L) - u_{3,1}(0)], \tag{13}$$

where Equation (9d) has been used. The current flowing out of this electrode is given by

$$I_3 = -\dot{Q}^e. \tag{14}$$

Consider time-harmonic motions with the following complex notation

$$(V_2, V_3, u_2, u_3, Q^e, I_3) = \text{Re}\left\{(\bar{V}_2, \bar{V}_3, U_2, U_3, \bar{Q}^e, \bar{I}_3) \exp(i\omega t)\right\}, \tag{15}$$

where $\bar{V}_2, \bar{V}_3, U_2, U_3, \bar{Q}^e$, and \bar{I}_3 are the complex amplitudes of V_2, V_3, u_2, u_3, Q^e , and I_3 . i is the imaginary unit. ω is the time-harmonic frequency. The electrodes at $x_3 = \pm b$ are connected by a circuit whose impedance is Z in harmonic motions, which provides the following circuit equation:

$$\bar{I}_3 = \bar{V}_3 / Z. \tag{16}$$

The substitution of Equations (12)–(15) into Equations (11) and (16) results in the following three equations for U_2, U_3 , and \bar{V}_3 :

$$-\bar{c}B_2U_{2,1111} + \rho A(\omega^2U_2 + i\omega 2\Omega U_3 + \Omega^2U_2) = 0, \tag{17a}$$

$$-\bar{c}B_3U_{3,1111} + \rho A(\omega^2U_3 - i\omega 2\Omega U_2 + \Omega^2U_3) = 0, \tag{17b}$$

$$\frac{\bar{V}_3}{Z} = -2i\omega c \left\{ \frac{L\epsilon_{11}\bar{V}_3}{2b} + f_{3113}[U_{3,1}(L) - U_{3,1}(0)] \right\}. \tag{17c}$$

Specifically, consider a simply supported beam with the following boundary conditions:

$$u_2(0, t) = u_3(0, t) = u_2(L, t) = u_3(L, t) = 0, \\ M_2(0, t) = M_3(0, t) = M_2(L, t) = M_3(L, t) = 0. \tag{18}$$

Equation (18) represents the simplest and most basic mounting of a beam, which was used in the first piezoelectric vibratory gyroscope [11]. The purpose of the present paper is to show that a vibrating flexoelectric beam can also operate as a gyroscope. Other mountings, such as a cantilever, can also be used, which changes the mathematical analysis but not the mechanism of the device. Therefore, other boundary conditions are not pursued here.

Equation (17a,b) form a system of linear ordinary differential equations. We look for its solution in the following form:

$$U_2 = \bar{U}_2 \exp(kx_1), U_3 = \bar{U}_3 \exp(kx_1) \tag{19}$$

where k is undetermined. The substitution of Equation (19) into Equation (17a,b) gives two linear homogeneous algebraic equations:

$$\begin{bmatrix} \rho A(\omega^2 + \Omega^2) - \bar{c}B_2k^4 & 2\rho Ai\omega\Omega \\ -2\rho Ai\omega\Omega & \rho A(\omega^2 + \Omega^2) - \bar{c}B_3k^4 \end{bmatrix} \begin{Bmatrix} \bar{U}_2 \\ \bar{U}_3 \end{Bmatrix} = \begin{Bmatrix} 0 \\ 0 \end{Bmatrix}. \tag{20}$$

For nontrivial solutions, the determinant of the coefficient matrix has to vanish, i.e.,

$$(\bar{c})^2 B_2 B_3 k^8 - \rho A(\omega^2 + \Omega^2) \bar{c}(B_2 + B_3)k^4 + [\rho A(\omega^2 + \Omega^2)]^2 + (2\rho Ai\omega\Omega)^2 = 0. \tag{21}$$

Equation (21) is a polynomial equation for k . We denote its eight roots by $k^{(N)}$, where $N = 1, 2, \dots, 8$. The corresponding nontrivial solutions of U_2 and U_3 are denoted by

$$\begin{Bmatrix} U_2 \\ U_3 \end{Bmatrix} = \begin{Bmatrix} 2\rho A i \omega \Omega \\ -[\rho A(\omega^2 + \Omega^2) - \bar{c} B_2 (k^{(N)})^4] \end{Bmatrix}. \tag{22}$$

Then, the general solution of Equation (17a,b) can be written as

$$\begin{aligned} U_2 &= \sum_{N=1}^8 (2\rho A i \omega \Omega) \bar{U}^{(N)} \exp(k^{(N)} x_1), \\ U_3 &= - \sum_{N=1}^8 [\rho A(\omega^2 + \Omega^2) - \bar{c} B_2 (k^{(N)})^4] \bar{U}^{(N)} \exp(k^{(N)} x_1), \end{aligned} \tag{23}$$

where $\bar{U}^{(N)}$ are undetermined constants. The substitution of Equation (23) into Equations (17c) and (18) yields nine linear algebraic equations for $\bar{U}^{(N)}$ and \bar{V}_3 . These equations are solved on a computer using MATLAB R2021a (Xi'an, China).

5. Numerical Results and Discussion

As a numerical example, consider a ceramic beam of BaTiO₃ that is not poled and hence is nonpiezoelectric. The relevant material constants are $C_{11} = 166$ GPa, $C_{12} = 77$ GPa, $C_{13} = 78$ GPa, $C_{33} = 162$ GPa, $C_{44} = 43$ GPa, $\epsilon_{33} = \epsilon_{22} = 12.6 \times 10^{-9}$ C²/(N·m²), and $f_{3113} = 10^{-6}$ N/C. The elastic and dielectric constants are from [25]. The flexoelectric constant is from [18,26]. Examples of other materials that have been used for micro-beams are zinc oxide, barium sodium niobate, barium titanate [27], and strontium titanate [28], which, when unpoled, may be considered for flexoelectric gyroscope applications. In [29], a micro-beam of BaTiO₃ with dimensions of 1.5, 3.2, and 11 μm was fabricated for experimental investigation. For our modeling analysis with the goal of demonstrating the basic operation of the gyroscope, the geometric parameters were chosen to be $a = b = 5$ μm , $c = d = a/2$, and $L = 200$ μm . Material damping is described by complex elastic constants $C_{pq}(1 + i/Q)$ with $Q = 10^2$. The amplitude of the driving voltage is $V_2 = 100$ volts. $Z = \infty$ is used for the open circuit output voltage. $\Omega = 3.6 \times 10^4$ rad/s, which is much smaller than (approximately 1%) the first resonance frequency of the beam, which is 3.6×10^6 rad/s. Some of these parameters may be varied separately below. We introduced Z_2 as a unit for Z :

$$Z_2 = \frac{1}{2i\omega c C_2}, \quad C_2 = \frac{L\epsilon_{11}}{2b}. \tag{24}$$

Figure 2a shows $|u_2(L/2)|$ versus the driving frequency ω with three resonances. The third one is barely visible. For gyroscope application, we are mainly interested in the first resonance. $|u_2(L/2)|$, $|u_3(L/2)|$ and the output voltage $|V_3|$ near the first resonance are shown in Figure 2b–d, respectively. u_2 is driven by the applied V_2 through flexoelectric coupling and is called the primary motion. u_3 is due to the Coriolis force associated with Ω and is called the secondary motion. V_3 is produced by u_3 through flexoelectric coupling. They all assume double-peak resonances because of flexural vibrations in both directions, which is typical for vibratory piezoelectric gyroscopes.

Figure 3 shows the effects of various parameters on the output voltage near the first resonance. Figure 3a shows that a larger flexoelectric coefficient leads to a higher output, which is as expected. Figure 3b shows that the output voltage drops when the cross section deviates somewhat from a square. This is because, for a beam with a cross section not close to a square, the resonance frequencies of flexural vibrations in the x_2 and x_3 directions are not close. Hence, the gyroscope is not working in the optimal condition (the so-called double-resonant condition). Figure 3c shows that, when the impedance of the output circuit increases, the output voltage increases too. At the same time, the output current decreases correspondingly. Figure 3d shows that the output voltage is linear in Ω when Ω is small,

which is ideal for angular rate sensing. For large values of Ω , the linearity is lost because Ω appears in Equation (17) in a complicated and nonlinear way.

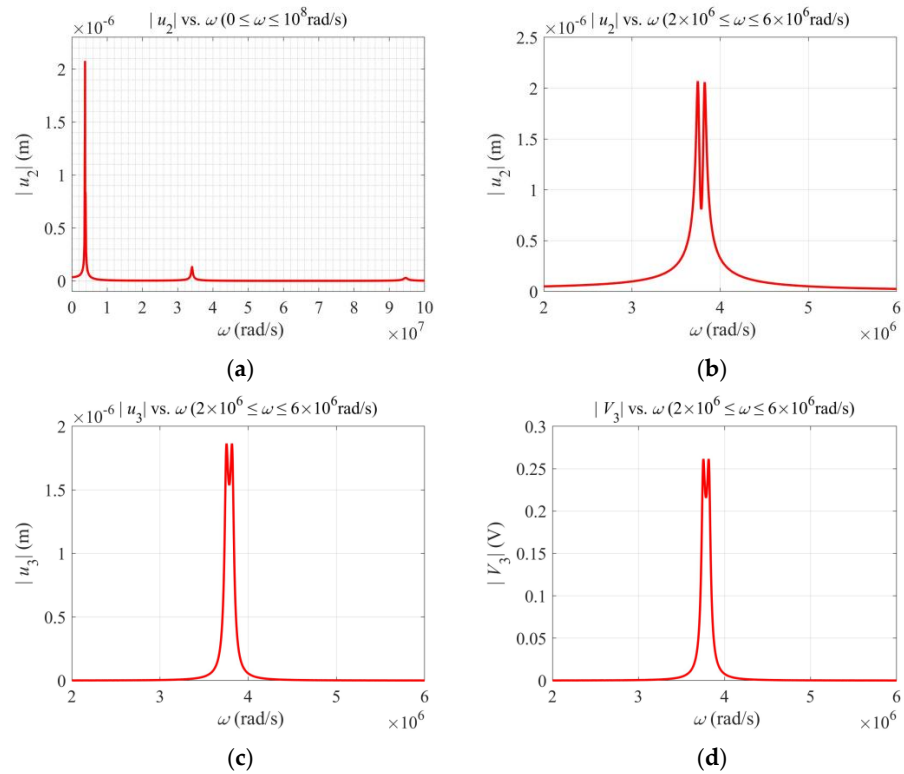


Figure 2. Behavior near the first resonance. (a) Primary motion showing resonances. (b) Primary motion near the first resonance. (c) Secondary motion near the first resonance. (d) Output voltage near the first resonance.

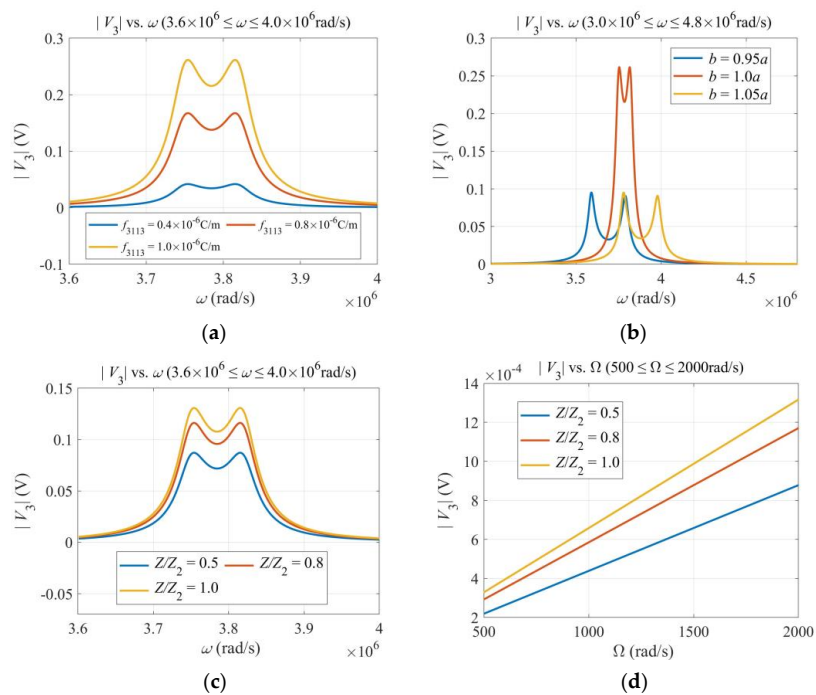


Figure 3. Effects of various parameters. (a) Flexoelectric coefficient. (b) Dimensions of the cross section. (c) Impedance of the output circuit. (d) Angular rate Ω . $\omega = 3.7 \times 10^6$ rad/s.

The output signal V_3 for detecting Ω depends on several physical and geometric parameters; in particular, the driving frequency ω and the impedance Z of the output circuit as shown in Figures 2 and 3, where ω and Z were varied one at a time. For a more comprehensive understanding of the behavior of the gyroscope, we plot V_3 versus ω and Ω together in Figure 4a, and V_3 versus ω and Z in Figure 4b, respectively. The curves in Figures 2 and 3 are formed by intersections of the surfaces in Figure 4 with different vertical planes. It can be seen from Figure 4a that, when Ω is fixed, there are two peaks as ω varies. The two peak values increase with Ω monotonically when Ω is small and saturate when Ω is large. The distance between the two peaks also increases with Ω . In Figure 4b, when Z is fixed, there are two peaks as ω varies. The two peak values increase with Z monotonically. When Z is small, the output circuit is nearly shorted, with a small V_3 . When Z is large, the output circuit is nearly open, with a large and saturated V_3 . These agree with Figure 3c,d.

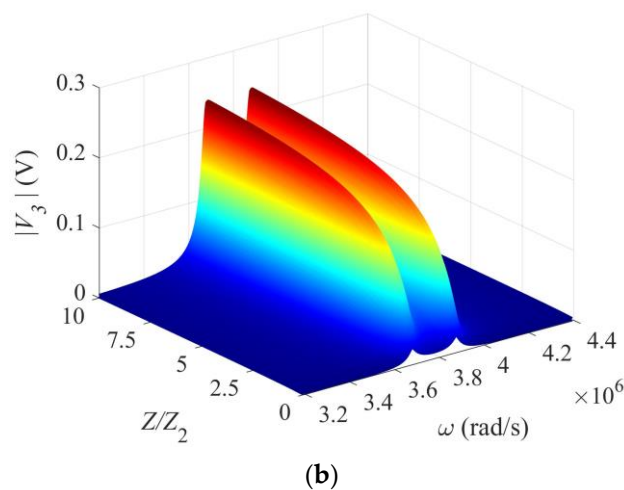
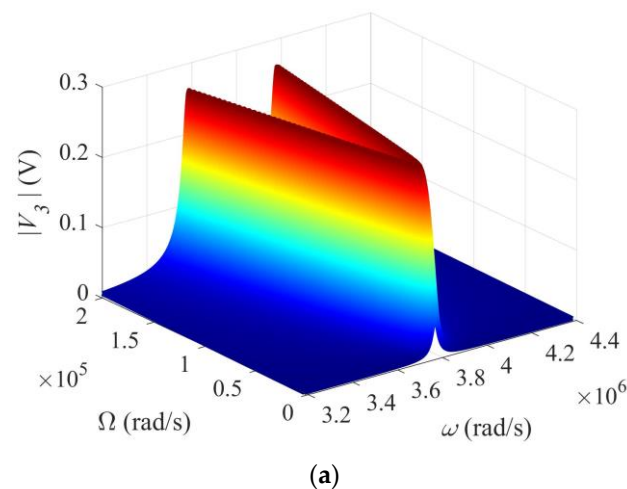


Figure 4. Three-dimensional views of the output voltage. (a) V_3 versus ω and Ω . $Z = \infty$. (b) V_3 versus ω and Z . $\Omega = 105$ rad/s.

6. Conclusions

It is shown theoretically that a micro-beam in flexural vibrations excited and detected flexoelectrically can be used to make a gyroscope to detect an angular rate. Compared to conventional piezoelectric beam gyroscopes, the flexoelectric beam gyroscope proposed has a simpler structure or electrode configuration. The one-dimensional model developed is effective in describing the basic behaviors of the beam flexoelectric gyroscope.

Author Contributions: Conceptualization, J.Y.; methodology, J.Y. and Y.Q.; software, Y.Q.; validation, Y.Q.; formal analysis, Y.Q.; investigation, Y.Q.; resources, F.J. and Y.Q.; data curation, Y.Q.; writing—original draft preparation, J.Y.; writing—review and editing, J.Y.; visualization, Y.Q.; supervision, F.J.; project administration, F.J.; funding acquisition, F.J. and Y.Q. All authors have read and agreed to the published version of the manuscript.

Funding: This research was funded by the National Natural Science Foundation of China (No. 12072253, Feng Jin), 111 Project version 2.0 (Feng Jin), and the Fundamental Research Funds for the Central Universities (xzy022020016, Yilin Qu).

Data Availability Statement: Not applicable.

Conflicts of Interest: The authors declare no conflict of interest. The funders had no role in the design of the study; in the collection, analyses, or interpretation of data; in the writing of the manuscript; or in the decision to publish the results.

References

1. Burdess, J.S.; Harris, A.J.; Cruickshank, J.; Wood, D.; Cooper, G. A review of vibratory gyroscopes. *Eng. Sci. Edu. J.* **1994**, *3*, 249–254. [[CrossRef](#)]
2. Soderkvist, J. Micromachined gyroscopes. *Sens. Actuators A* **1994**, *43*, 65–71. [[CrossRef](#)]
3. Yang, J.S. A review of analyses related to vibrations of rotating piezoelectric bodies and gyroscopes. *IEEE Trans. Ultrason. Ferroelect. Freq. Contr.* **2005**, *52*, 698–706. [[CrossRef](#)] [[PubMed](#)]
4. Loveday, P.W. Analysis and Compensation of Imperfection Effects in Piezoelectric Vibratory Gyroscopes. Ph.D. Dissertation, Virginia Polytechnic Institute and State University, Blacksburg, VA, USA, 1999.
5. Fang, H.Y. Vibrations of a Rotating Piezoelectric Body and Applications in Gyroscopes. Ph.D. Dissertation, University of Nebraska–Lincoln, Lincoln, NE, USA, 2000.
6. Liang, F.; Liang, D.D.; Qian, Y.J. Dynamical analysis of an improved MEMS ring gyroscope encircled by piezoelectric film. *Int. J. Mech. Sci.* **2020**, *187*, 105915. [[CrossRef](#)]
7. Hodjat-Shamami, M.; Ayazi, F. Eigenmode operation of piezoelectric resonant gyroscopes. *Microsyst. Nanoeng.* **2020**, *6*, 108. [[CrossRef](#)] [[PubMed](#)]
8. Obitani, K.; Qian, J.; Tsuchiya, T.; Araya, K.; Yachi, M. Electrode design of single crystal lithium niobate piezoelectric disk gyroscope. In Proceedings of the 2020 IEEE International Symposium on Inertial Sensors and Systems (INERTIAL), Hiroshima, Japan, 23–26 March 2020; pp. 1–2.
9. Qu, T.; Zhou, G.; Xue, X.; Teng, J. Cylindrical shell vibration gyroscope excited and detected by high-temperature-sintered piezoelectric ceramic electrodes. *Sensors* **2020**, *20*, 5972. [[CrossRef](#)] [[PubMed](#)]
10. Larkin, K.; Ghommem, M.; Serrano, M.; Abdelkefi, A. A review on vibrating beam-based micro/nano-gyroscopes. *Microsyst. Technol.* **2021**, *27*, 4157–4181. [[CrossRef](#)]
11. Gates, W.D. Vibrating angular rate sensor may threaten the gyroscope. *Electronics* **1968**, *41*, 130–134.
12. Soderkvist, J. Piezoelectric beams and vibrating angular rate sensors. *IEEE Trans. Ultrason. Ferroelect. Freq. Contr.* **1991**, *38*, 271–280. [[CrossRef](#)]
13. Yang, J.S.; Fang, H.Y. Analysis of a rotating elastic beam with piezoelectric films as an angular rate sensor. *IEEE Trans. Ultrason. Ferroelect. Freq. Contr.* **2002**, *49*, 798–804. [[CrossRef](#)] [[PubMed](#)]
14. Sahin, E.; Dost, S. A strain-gradients theory of elastic dielectrics with spatial dispersion. *Int. J. Engng. Sci.* **1988**, *26*, 1231–1245. [[CrossRef](#)]
15. Tagantsev, A.K. Piezoelectricity and flexoelectricity in crystalline dielectrics. *Phys. Rev. B* **1986**, *32*, 5883–5889. [[CrossRef](#)] [[PubMed](#)]
16. Shen, S.; Hu, S. A theory of flexoelectricity with surface effect for elastic dielectrics. *J. Mech. Phys. Solids* **2010**, *58*, 665–677. [[CrossRef](#)]
17. Zhang, R.; Liang, X.; Shen, S. A Timoshenko dielectric beam model with flexoelectric effect. *Meccanica* **2015**, *51*, 1181–1188. [[CrossRef](#)]
18. Zhou, Z.D.; Yang, C.P.; Su, Y.X.; Huang, R.; Lin, X.L. Electromechanical coupling in piezoelectric nanobeams due to the flexoelectric effect. *Smart Mater. Struct.* **2017**, *26*, 095025. [[CrossRef](#)]
19. Hu, Y.T.; Wang, J.N.; Yang, F.; Xue, H.; Hu, H.P.; Wang, J. The effect of first-order strain gradient in micro piezoelectric-bimorph power harvester. *IEEE Trans. Ultrason. Ferroelect. Freq. Contr.* **2011**, *58*, 849–852.
20. Qu, Y.L.; Jin, F.; Yang, J.S. Buckling of flexoelectric semiconductor beams. *Acta Mech.* **2021**, *232*, 2623–2633. [[CrossRef](#)]
21. Yang, W.J.; Liang, X.; Shen, S.P. Electromechanical responses of piezoelectric nanoplates with flexoelectricity. *Acta Mech.* **2015**, *226*, 3097–3110. [[CrossRef](#)]
22. Ray, M.C. Mesh free model of nanobeam integrated with a flexoelectric actuator layer. *Compos. Struct.* **2017**, *159*, 63–71. [[CrossRef](#)]
23. Fan, M.; Min, H. Active actuating of a simply supported beam with the flexoelectric effect. *Materials* **2020**, *13*, 1735. [[CrossRef](#)]
24. Mase, G.T.; Mase, G.E. *Continuum Mechanics for Engineers*, 2nd ed.; CRC Press: Boca Raton, FL, USA, 1990.

25. Auld, B.A. *Acoustic Fields and Waves in Solids*; Wiley: New York, NY, USA, 1973.
26. Shu, L.; Wei, X.; Pang, T.; Yao, X.; Wang, C. Symmetry of flexoelectric coefficients in crystalline medium. *J. Appl. Phys.* **2011**, *110*, 104106. [[CrossRef](#)]
27. Zaki, N.A.F.; Aziz, A.A.; Khairudin, N.; Burham, N. Simulation of zinc oxide, barium sodium niobate, and barium titanate as lead-free piezoelectric materials. In Proceedings of the 2021 IEEE Regional Symposium on Micro and Nanoelectronics (RSM), Kuala Lumpur, Malaysia, 2–4 August 2021; pp. 38–41.
28. Bhaskar, U.; Banerjee, N.; Abdollahi, A.; Wang, Z.; Schlom, D.G.; Rijnders, G.; Catalan, G. A flexoelectric microelectromechanical system on silicon. *Nat. Nanotech.* **2016**, *11*, 263–266. [[CrossRef](#)] [[PubMed](#)]
29. Yamaguchi, H.; Tatami, J.; Iijima, M. Measurement of mechanical properties of BaTiO₃ layer in multilayered ceramic capacitor using a microcantilever beam specimen. *J. Ceram. Soc. Jpn.* **2019**, *127*, 335–338 2019. [[CrossRef](#)]